AIP Journal of Applied Physics

Argon-ion-induced formation of nanoporous GaSb layer: Microstructure, infrared luminescence, and vibrational properties

D. P. Datta, A. Kanjilal, B. Satpati, S. Dhara, T. D. Das, D. Kanjilal, and T. Som

Citation: Journal of Applied Physics **116**, 033514 (2014); doi: 10.1063/1.4890608
View online: http://dx.doi.org/10.1063/1.4890608
View Table of Contents: http://scitation.aip.org/content/aip/journal/jap/116/3?ver=pdfcov
Published by the AIP Publishing

Argon-ion-induced formation of nanoporous GaSb layer: Microstructure, infrared luminescence, and vibrational properties

D. P. Datta,[1] A. Kanjilal,[2] B. Satpati,[3] S. Dhara,[4] T. D. Das,[5] D. Kanjilal,[6] and T. Som[1,a)]
[1]*SUNAG Laboratory, Institute of Physics, Bhubaneswar, Odisha 751 005, India*
[2]*Department of Physics, Shiv Nadar University, Uttar Pradesh 201 314, India*
[3]*Surface Physics and Material Science Division, Saha Institute of Nuclear Physics, 1/AF Bidhannagar, Kolkata 700 064, India*
[4]*Surface and Nanoscience Division, Materials Science Group, Indira Gandhi Centre for Atomic Research, Kalpakkam 603 102, India*
[5]*Department of Electronic Science, University of Calcutta, APC Road, Kolkata 700 009, India*
[6]*Inter-University Accelerator Centre, Aruna Asaf Ali Marg, New Delhi 110 067, India*

(Received 27 June 2014; accepted 8 July 2014; published online 18 July 2014)

Room temperature implantation of 60 keV Ar^+-ions in GaSb to the fluences of 7×10^{16} to 3×10^{18} ions cm^{-2} is carried out at two incidence angles, viz 0° and 60°, leading to formation of a nanoporous layer. As the ion fluence increases, patches grow on the porous layer under normal ion implantation, whereas the porous layer gradually becomes embedded under a rough top surface for oblique incidence of ions. Grazing incidence x-ray diffraction and cross-sectional transmission electron microscopy studies reveal the existence of nanocrystallites embedded in the ion-beam amorphized GaSb matrix up to the highest fluence used in our experiment. Oxidation of the nanoporous layers becomes obvious from x-ray photoelectron spectroscopy and Raman mapping. The correlation of ion-beam induced structural modification with photoluminescence signals in the infrared region has further been studied, showing defect induced emission of additional peaks near the band edge of GaSb. © *2014 AIP Publishing LLC*. [http://dx.doi.org/10.1063/1.4890608]

I. INTRODUCTION

GaSb nanostructures are considered to be promising for low power electronic and optoelectronic devices operating in near to mid-infrared wavelength range, owing to low band gap and high carrier mobility of GaSb.[1] For instance, GaSb nanowires were utilized to fabricate single electron transistor and infrared laser.[2,3] In addition to several techniques used to develop GaSb nanostructures,[4,5] a porous layer containing nanofibers has been developed in GaSb by ion-beam irradiation with energy in the range of tens of keV to a few MeV.[6–13] Interestingly, the diameters of these nanofibers are found to be in the range of 15–25 nm, irrespective of the energy of the incident ions, whereas the thickness of the nanoporous layer becomes an order of magnitude higher than the range of ions with increasing fluence.[6–13] The experimental investigations on porous structures formed in the low fluence regime ($<10^{16}$ ions cm^{-2}) have shown residual crystallinity in the nanofibers.[8,10] It is, however, imperative to explore whether nanocrystallites exist within the nanofibers for fluences having orders of magnitude higher than those reported earlier. This is predominantly significant in the context of luminescence properties due to band-gap opening with decreasing crystallite size.[14] Crystalline GaSb is known to exhibit photoluminescence (PL) in the infrared region (700–800 meV) due to the radiative recombination of excitons via band gap transitions.[15–19] On the other hand, PL emission in 785–805 meV was reported for GaSb nanowires.[20] Moreover, visible range PL was reported for focused ion-beam produced nanoporous structures (after post-implantation annealing).[11] Thus, the existence of nanocrystallites in ion-induced porous layer can significantly influence the PL emission from GaSb. Moreover, GaSb surface is prone to oxidation owing to the reactive nature of Ga and Sb.[21] In fact, medium energy ion-beam induced formation of Ga_2O_3 and Sb_2O_3 at room temperature (RT) on the nanoporous structures was confirmed in our previous report.[12,13] The PL emission from a nanoporous GaSb structure in presence of these oxides is yet to be explored and understood, particularly for structures generated by ion fluences orders of magnitude higher from the previous studies.[11]

In this paper, we report the structural, compositional, vibrational, and luminescence properties of the nanoporous GaSb layers containing nanocrystallites, evolved under 60 keV Ar^+-ion implantation with fluences in the range of $7 \times 10^{16} - 3 \times 10^{18}$ ions cm^{-2}. Subsequent to the demonstration of formation of a porous structure by scanning electron microscopy (SEM), the presence of nanocrystallites embedded in the amorphous matrix will be shown by grazing incidence x-ray diffraction (GIXRD) and transmission electron microscopy (TEM) studies. Presence of Ga_2O_3 and Sb_2O_3 phases in the porous layer will be demonstrated by x-ray photoelectron spectroscopy (XPS) and Raman mapping. Using PL spectroscopy, we will show infrared emission from such nanoporous structures and attempt to correlate the emission with band gap opening due to quantum confinement in the nanocrystallites.

II. EXPERIMENTAL

Mirror polished, *p*-type GaSb(100) substrates (area 1×1 cm^2) were ultrasonically cleaned by using trichloroethylene,

a)Author to whom correspondence should be addressed. Electronic mail: tsom@iopb.res.in

acetone, ethanol, and de-ionized water and exposed to 60 keV Ar^+-ions at RT with fluences in the range of 7×10^{16} to 3×10^{18} ions cm^{-2}. Two ion incidence angles (viz 0° and 60°) were chosen for the present experiments. Implantation-induced evolution of microstructures was characterized by using both SEM [Carl-Zeiss] and cross-sectional transmission electron microscopy (XTEM) [field emission gun based 300 keV FEI Tecnai G^2 S-Twin]. In addition, crystalline nature of ion-irradiated samples was examined by employing GIXRD (5°) measurements [D8-Discover, Bruker] using the Cu-K_α radiation ($\lambda = 1.54$ Å) which was further corroborated by selected area electron diffraction (SAED) during TEM studies. Furthermore, surface chemical composition was examined by XPS [VG Instruments] using Mg-K_α radiation ($h\nu = 1254$ eV). Raman mapping was performed at RT by using the 514 nm line of an Ar^+-ion laser [inVia, Renishaw] and the data were recorded with the help of a 1800 lines nm^{-1} grating and a thermoelectrically cooled CCD detector. The spectra were recorded in the backscattering geometry by using a 100× objective with N.A. value of 0.85. The fully automated motorized sample stage (Renishaw MS20), having a spatial resolution of 100 nm, was used for Raman imaging. This was performed by integrating intensities, which is essentially the peak intensity distribution corresponding to a particular mode frequency collected over a pre-defined area and grid resolution. In the present study, a total area of $2 \times 2\ \mu m^2$ with $100 \times 600\ nm^2$ grid resolution is probed for the Raman mapping using the Stream Line imaging facility covering large area. Low-temperature PL spectra were collected at 12 K using 532 nm line of a diode pumped solid state laser with a surface power density of 1 W cm^{-2}.

III. RESULTS AND DISCUSSION

The plan-view SEM images in Figs. 1(a) and 1(b) show the surface morphology of Ar^+-ion implanted samples at $\theta = 60°$, whereas Figs. 1(c) and 1(d) illustrate the same corresponding to $\theta = 0°$ which depict the evolution of porous structures. As discerned from Figs. 1(a) and 1(c), corresponding to the lowest fluence of 7×10^{16} ions cm^{-2}, the porous layers comprise a network of nanofibers (diameter 15–25 nm). However, ridge-like structures are observed on top of the porous network for $\theta = 60°$, whereas terrace-like structures are developed on porous layer for $\theta = 0°$. The fluence-dependent evolution of nanoporous structures for $\theta = 60°$ further demonstrates the impact of off-normal irradiation. For instance, the porous layer gets embedded under a continuous rough top surface at higher ion fluences (at 60°) [Fig. 1(b)], whereas large patches are observed on top of the nanoporous layer under normal incidence [Fig. 1(d)]. It should be mentioned that a modulated interface of the nanoporous layer with the crystalline GaSb substrate underneath was discernible in the cross-sectional SEM images for the obliquely implanted samples.[12]

The presence of crystalline phases in the implantation-induced nanoporous structure is evident from the GIXRD data, where the spectra recorded from the samples implanted at 60° and 0° are shown as a function of fluence in Figs. 2(a) and 2(b), respectively. The collected spectra for both the angles exhibit characteristic diffraction peaks at $2\theta = 25.4°$,

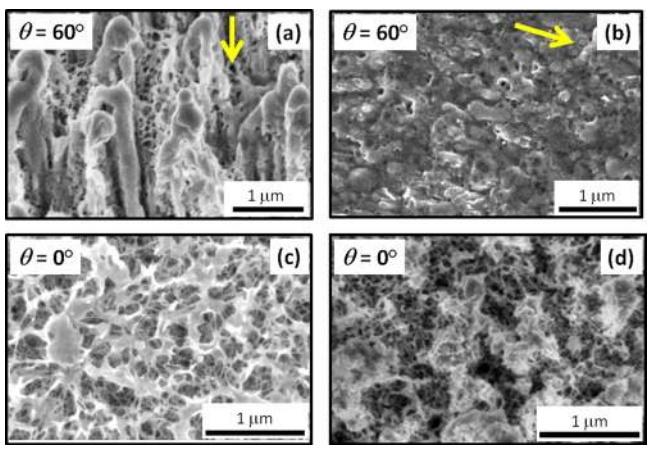

FIG. 1. Plan-view SEM images of GaSb surfaces: Implanted with obliquely incident ($\theta = 60°$) Ar^+-ions to the fluences of 7×10^{16} ions cm^{-2} (a) and 3×10^{18} ions cm^{-2} (b) and normally incident Ar^+-ions to the fluences of 7×10^{16} ions cm^{-2} (c) and 3×10^{18} ions cm^{-2} (d).

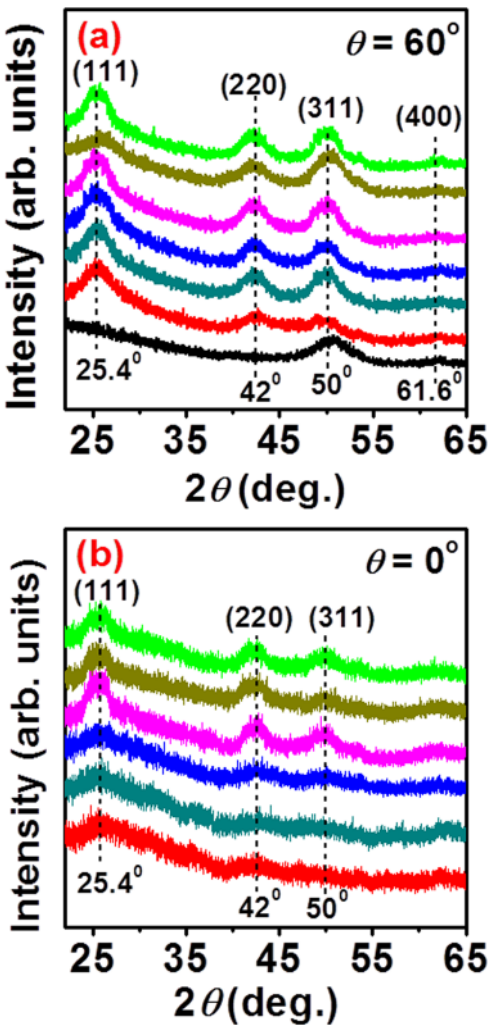

FIG. 2. GIXRD spectra of implanted GaSb samples: Ar^+-ions incident at an angle of 60° (a), and 0° (b), to the fluences of 7×10^{16} ions cm^{-2} (red), 1×10^{17} ions cm^{-2} (cyan), 4×10^{17} ions cm^{-2} (blue), 7×10^{17} ions cm^{-2} (magenta), 1×10^{18} ions cm^{-2} (dark yellow), and 3×10^{18} ions cm^{-2} (green). GIXRD data obtained from the pristine sample are also shown [black line in (a)] for comparison. The spectra were shifted along the *y*-direction for better clarity.

42°, and 50° which correspond to the (111), (200), and (311) reflections from the cubic GaSb crystalline structure.[22] Using the full width at half maximum (FWHM) of the (311) diffraction peak in the Scherrer's formula,[23] the average crystallite size has been estimated to be around 1.5–3.5 nm for both the incident angles. Results obtained from GIXRD are found to corroborate well with the findings of TEM analyses described below.

The XTEM images of the GaSb substrate implanted with the fluence of 7×10^{16} ions cm^{-2} at $\theta = 60°$ are shown in Fig. 3. The XTEM image in Fig. 3(a) confirms that a porous layer is formed at the top of the GaSb substrate. A micrograph of the porous layer, taken at lower magnification, is shown in Fig. 3(b). It is evident from Figs. 3(a) and 3(b) that the porous microstructure comprises nanofibers with darker patches on top. It is to be noted here that the XTEM images are taken perpendicular to the direction of the ion-beam injection [depicted by the yellow arrow in Fig. 1(a)] onto the surface. Thus, the dark patches are cross-sections of the ridge-like structures seen in Fig. 1(a). The modulated nature of the interface of the porous layer with the GaSb substrate underneath becomes clear from the XTEM image of Fig. 3(b), where the interface is indicated by a dashed yellow line. The presence of crystalline phases in the nanoporous layer, in the form of nanocrystallites, is recognized from the SAED patterns [shown in Figs. 3(c)–3(e)] obtained from three different regions marked as "1," "2," and "3" on Fig. 3(a). The SAED pattern from the top region of the porous layer, including the dark patches (region "1"), shows the presence of streaky bright spots in concentric rings, which can be indexed by the characteristic (002), $(11\bar{1})$, and $(02\bar{2})$ rings, originating from the fine and randomly distributed GaSb crystallites with cubic lattice structure.[24] However, the diffused rings in the background indicate the coexistence of amorphous materials as well. On the other hand, the SAED pattern obtained from region "2," containing both the porous layer and the substrate [Fig. 3(d)] shows an overlap of ordered spots from the unimplanted substrate on the diffused rings, passing through (002), $(11\bar{1})$, and $(02\bar{2})$ spots, from randomly oriented fine structures (as stated above). The SAED pattern taken from the substrate underneath the porous layer [Fig. 3(e)] exhibits ordered spots corresponding to a cubic GaSb single-crystalline structure along the [110] zone axis. In addition, the presence of crystalline pockets (where lattice fringes are discernible) within an amorphous matrix is obvious from the high-resolution TEM (HRTEM) image of the porous layer [Fig. 3(f)]. The *d*-spacing of the lattice fringes [inset in Fig. 3(f)] is measured to be 0.35 nm which matches well with the d_{111} of cubic GaSb. The size of the crystallites, determined from the HRTEM images, is somewhat higher than those estimated from the respective GIXRD patterns (described above). Similar to the above results, the presence of nanocrystallites embedded in an amorphous porous structure has also been detected in GaSb implanted with the highest fluence (3×10^{18} ions cm^{-2}) (image not shown).

The HRTEM image in Fig. 3(g) shows the interface region of the porous layer with the GaSb substrate underneath. While the substrate is single-crystalline, local presence of crystal-defects in the substrate can be observed below the interface (indicated by the yellow line). Moreover, high-angle annular dark field-scanning TEM (HAADF-STEM) image [Fig. 3(h)] reveals nanofiber-like structures sandwiched between a dense surface layer [the dark patches observed in Fig. 3(a)] and the unirradiated GaSb substrate [Fig. 3(h)]. The presence of small voids within these patches at the surface can also be seen in Fig. 3(h). In order to study the compositional variation across the porous layer, a series of energy dispersive x-ray spectroscopy (EDS) spectra were recorded along the vertical arrow shown on the STEM image [see Fig. 3(h)], which are shown in Fig. 3(i). A comparison of Figs. 3(h) and 3(i) shows that the concentration of O stays more or less constant as one goes from the underlying GaSb substrate towards the top surface. On the other hand, although the intensity of Ga and Sb counts stays constant within the substrate [up to ~70 nm from the origin, as shown

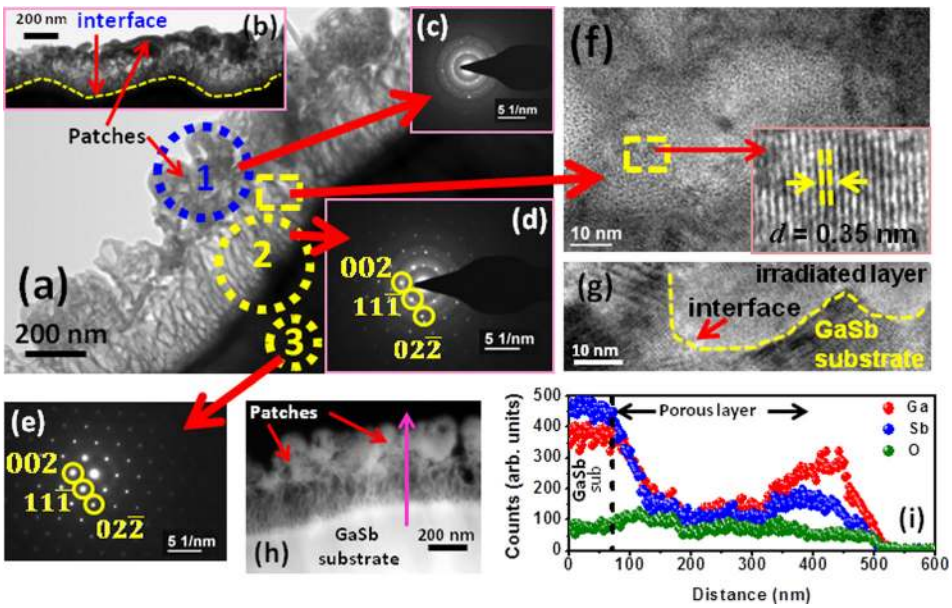

FIG. 3. (a) XTEM image of GaSb implanted to the fluence of 7×10^{16} cm^{-2} for obliquely incident ions at 60°, (b) low magnification TEM image showing the modulated interface. (c)–(e) present the SAED patterns collected from the regions marked by blue circles and identified as "1," "2," and "3" on the image, respectively. HRTEM images shown in (f) and (g) are obtained from the porous layer and the interface region, respectively. (h) HAADF-STEM image of the porous layer and (i) EDS spectra taken along the line shown on STEM image.

by the dotted black line in Fig. 3(i)], subsequent decrease is observed in the porous layer, followed by peaks at the top surface of the porous layer [within the ~400–500 nm region in Fig. 3(i)]. The decrease in Ga and Sb counts seems to be due to the porous nature of the layer, whereas the peaks near the top surface are due to denser patches observed in the XTEM and STEM images.

The porous microstructure generated by normal ion implantation to the highest fluence of 3×10^{18} ions cm^{-2} can be observed in the XTEM images of Fig. 4. It should be mentioned here that in our earlier XTEM studies on GaSb implanted with normally incident 60 keV Ar^{+}-ions to the fluence of 7×10^{16} ions cm^{-2},[13] an uniformly thick porous layer comprising nanofibers was observed. This nanofibrous layer contained nanocrystallites within an amorphous matrix[13] similar to obliquely incident ion implanted porous GaSb in the present experiment (described above). The evolution of such uniformly thick nanofibrous layer at higher fluence can be followed from the representative XTEM image presented in Fig. 4(a). The micrograph in Fig. 4(a) shows the formation of large voids (dimensions > 200 nm) in the top region of the nanoporous layer. Dimension of the voids decreases towards the interface of the porous layer with the substrate underneath. However, a few small voids are also observed in the top region, as indicated in Fig. 4(a). The presence of nanofibers in the porous layer can be confirmed both from the micrograph as well as from the HAADF-STEM image shown in Fig. 4(b). In addition, modulations at the interface of the porous layer with the underlying crystalline substrate are discernible in Fig. 4(a) (indicated by the dashed yellow line). The EDS line scans [taken along the line shown in Fig. 4(b)] shown in Fig. 4(c) shows O absorption in the layer in addition to a higher count of Ga in the porous layer compared with Sb. On the other hand, the SAED pattern in Fig. 4(d), obtained from the porous layer [the yellow circle marked as "1" in Fig. 4(a)] shows an overlap of concentric diffraction spots (representative of a polycrystalline phase containing randomly oriented crystallites) with ordered diffraction spots [indexed as (002), $(11\bar{1})$, and $(02\bar{2})$ spots]. The presence of concentric diffraction spots in the SAED pattern confirms existence of nanocrystallites within the porous layer, even after application of fluence as high as 3×10^{18} ions cm^{-2}. The HRTEM image of the porous layer in Fig. 4(e) also shows the presence of crystalline phase at this fluence (lattice fringes are observed all over the structure).

The chemical state of the O absorbed in the porous layer becomes clear from the XPS analyses. XPS spectra recorded from the irradiated GaSb substrates with fluences of 7×10^{16} and 3×10^{18} ions cm^{-2} at $\theta = 60°$ and 0° are shown in Figs. 5(a) and 5(b), respectively, for comparison. Peaks observed in the Ga *3d* spectra at 19.06, 20.26, and 23.1 eV can be assigned to Ga-Sb bonds in GaSb, Ga-O bonds in Ga_2O_3, and O-Ga bonds due to O *2s* state, respectively.[25,26] The corresponding Sb *3d* spectra were deconvoluted into Sb-Ga bonds in GaSb (527.1 eV), Sb-Sb bonds in elemental Sb (528.3 eV), and Sb-O bonds in Sb_2O_3 (530.1 eV) with a spin-orbit splitting of 9.4 eV.[27–30] The peak observed at 531.1 eV for Sb $3d_{5/2}$ spectrum corresponds to O *1s*. The XPS results confirm the formation of Ga_2O_3 and Sb_2O_3 phases at the nanostructure surface via oxygen absorption.

In order to further investigate the spatial distribution of the oxide phase over the porous microstructure, we carried out the Raman mapping of the implanted GaSb. The peaks selected for Raman mapping were around 220–224 cm^{-1} and 143–154 cm^{-1} which correspond to longitudinal optical mode (LO) of GaSb[30,31] and β-Ga_2O_3[32,33] phases, respectively. The distributions of GaSb and β-Ga_2O_3, as detected by Raman mapping, are presented in Figs. 6(a)–6(c) and Figs. 6(d)–6(f), respectively, as a function of ion fluence and angles of incidence. A comparison of morphology of the nanoporous layer seen in the SEM images [Figs. 1(a), 1(b), and 1(d)] with those of Figs. 6(a)–6(f) confirms the formation of β-Ga_2O_3 over the nanoporous structures. It may be

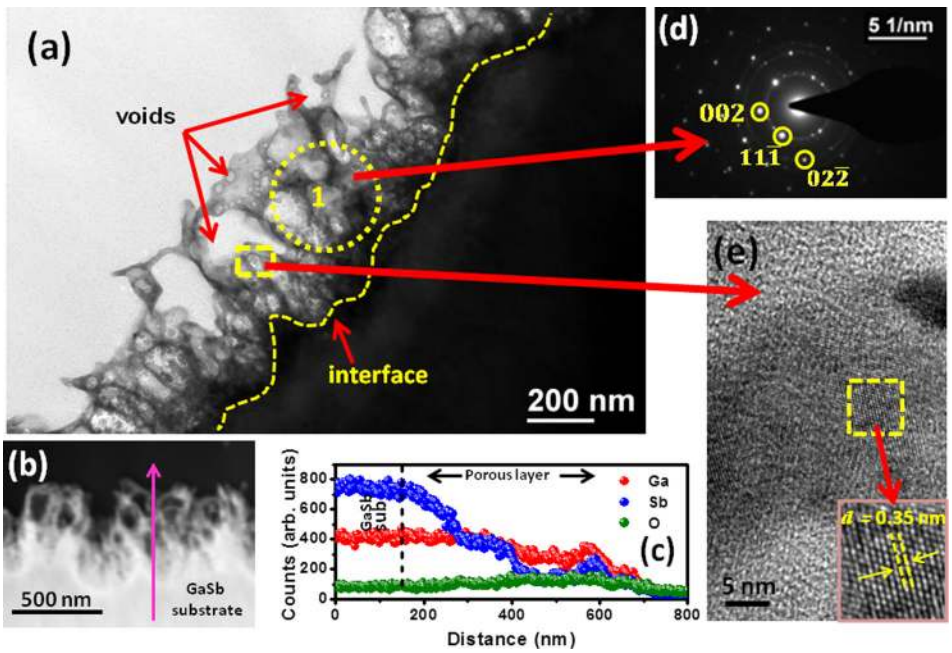

FIG. 4. (a) XTEM image of normally implanted GaSb samples to the fluence of 3×10^{18} ions cm^{-2}, (b) HAADF-STEM image of the porous layer, (c) EDS spectra collected along the arrow shown on the STEM image, (d) SAED pattern obtained from the region of the porous layer marked by the yellow circle in (a), and (e) HRTEM image obtained from the porous layer.

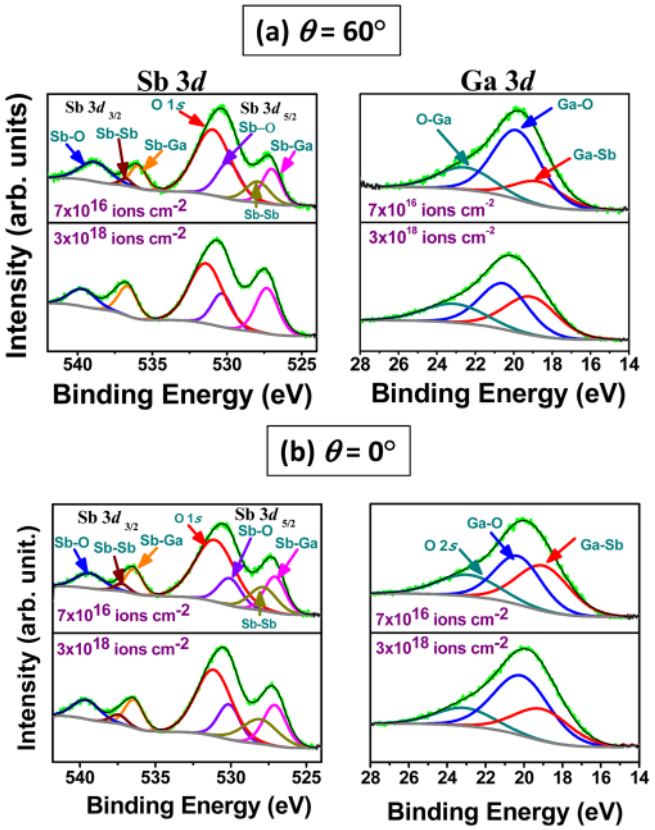

FIG. 5. Sb 3*d* and Ga 3*d* XPS spectra corresponding to the implanted samples to the fluences of 7×10^{16} and 3×10^{18} ions cm^{-2}: $\theta = 60°$ (a) and $\theta = 0°$ (b). The corresponding microstructures are shown in Figs. 1(a)–1(d).

noted that the Raman mappings of GaSb and β-Ga_2O_3 obtained from the porous layer formed at the highest fluence of 3×10^{18} ions cm^{-2} at $\theta = 60°$, show a network structure [Figs. 6(b) and 6(e)] that corresponds to the nanofibers below the rough top surface developed under oblique ion incidence [see Fig. 1(b)]. This result further fortifies the oxidation of the nanoporous structure embedded under the rough top layer (as described above).

To investigate the influence of implantation-induced structural and compositional modifications (described above) on the luminescence of GaSb, PL emission from the implanted samples was recorded at 12 K [Figs. 7(a)–7(d)]. In order to elucidate the impact of microstructure, the PL spectrum of the pristine GaSb was recorded [see inset of Fig. 1(a)], showing a peak at ~778 meV. However, the PL spectra recorded from the irradiated GaSb substrates show a broad peak in the range of 780–785 meV. All the recorded PL spectra were deconvoluted using a standard fitting procedure, where four different components are highlighted under the curve in each spectrum [Figs. 7(a)–7(d)]. It appears that even for the lowest ion fluence of 7×10^{16} ions cm^{-2} at $\theta = 60°$, the PL spectrum consists of four bands peaking at 784.1, 786, 788.6, and 790.3 meV [Fig. 7(a)]. When the ion fluence increases to 3×10^{18} ions cm^{-2}, these peaks are found to generally get blue shifted at 784.9, 786, 789.1, and 790.6 meV, respectively [Fig. 7(b)]. On the other hand, for $\theta = 0°$, these four peaks are found to appear at 782.8, 784.4, 788.5, and 790.4 meV at the lowest fluence of 7×10^{16} ions cm^{-2} [Fig. 7(c)], while they are also generally blue shifted to 783.8, 785.4, 789.1, and 790.3 meV, respectively, at the highest fluence of 3×10^{18} ions cm^{-2} [Fig. 7(d)].

In is known that the oxide phases like β-Ga_2O_3 are luminescent in the visible range.[34–36] On the other hand, since the near-band transition mediated emission of a single peak at 778 meV[15,18] is observed in the pristine GaSb [inset, Fig. 7(a)], the blue-shifted PL bands in the region 780–795 meV, as observed for the ion implanted samples, are likely to be

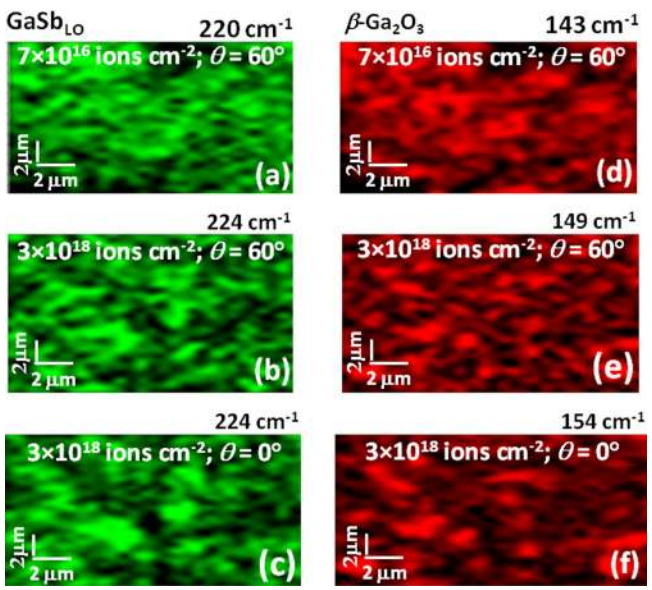

FIG. 6. Raman mapping data of GaSb and β-Ga_2O_3 taken over the Ar^+-ion implanted porous GaSb structures: (a) 7×10^{16} ions cm^{-2}; $\theta = 60°$, (b) 3×10^{18} ions cm^{-2}; $\theta = 60°$, (c) 7×10^{16} ions cm^{-2}; $\theta = 0°$, (d) 7×10^{16} ions cm^{-2}; $\theta = 60°$, (e) 3×10^{18} ions cm^{-2}; $\theta = 60°$, (f) 7×10^{16} ions cm^{-2}; $\theta = 0°$. The corresponding microstructures are shown in Figs. 1(a), 1(b), and 1(d).

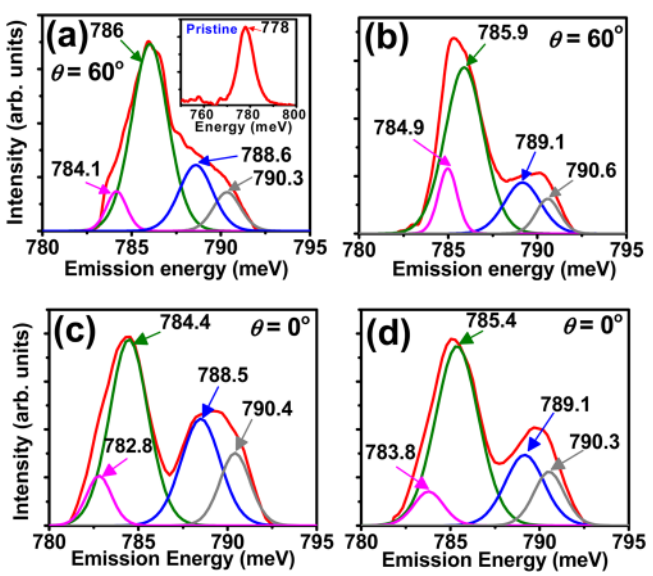

FIG. 7. PL spectra obtained from GaSb samples implanted with 60 keV Ar^+-ions incident at $\theta = 60°$ to the ion fluences of 7×10^{16} ions cm^{-2} (a), 3×10^{18} ions cm^{-2} (b). The same recorded from samples implanted by normally incident ($\theta = 0°$) ions to the fluences of 7×10^{16} cm^{-2} (c) and 3×10^{18} cm^{-2} (d). The spectra were collected at 12 K using 532 nm line of a diode pumped solid state laser.

associated with the GaSb nanocrystallites[15–20] embedded in an amorphous matrix. Earlier observations of PL emission from GaSb, in the range of 770–800 meV, were discussed in terms of donor-acceptor pair transitions and bound excitonic transitions.[15–20] In fact, the PL line observed around 779 meV is usually assigned to a donor-acceptor pair transition (denoted as A band), involving the neutral state of the native acceptor.[15,18] Although Iyer *et al.* showed that the peak can shift to 780 meV for highly doped GaSb,[17] this cannot be the case in the present scenario since the GaSb wafers are undoped. Meanwhile, the peak observed at around 784.4 meV was also observed by Iyer *et al.* but the origin of this peak was unidentified.[16] Bosacchi *et al.* also reported a PL peak at 788 meV from crystalline bulk GaSb which was correlated to a donor to carbon pair recombination.[18] On the other hand, Ploog *et al.* recorded a PL peak at 784 meV from a quantum well structure of GaSb and correlated it to electron-heavy hole transition.[19] In addition, Jeppsson *et al.* demonstrated a dominant PL peak between 785 and 800 meV for GaSb nanowire structures,[20] although the origin of the radiative transition could not be identified. A comparison between PL spectra obtained in the present case with those reported earlier, especially, with PL emission from nanoscale structures,[19,20] indicates that the observed blue shift in the PL emission can be attributed to three-dimensional quantum confinement in GaSb nanocrystallites due to the opening of the effective band gap by decreasing the average crystallite size[37] with increasing ion fluence. This is further confirmed by the XTEM studies (only a few nanometers) showing the formation of nanocrystallites with sizes smaller than the Bohr radius of GaSb, namely, 20.48 nm.[11] However, the insignificant difference in PL peak positions in Figs. 7(a) and 7(b), namely, 786 and 785.9 meV (corresponding to fluences of 7×10^{16} and 3×10^{18} ions cm^{-2} at $\theta = 60°$, respectively) is not clear yet, but looking at blue shifts in other PL peak positions, it seems that the peak residing at 786 meV is originating from radiative defect centers. The blue shift from 784.4 to 785.4 meV, observed in Figs. 7(c) and 7(d), corresponding to $\theta = 0°$, can be associated with a decrease in average crystallite size with increasing ion fluence. We should note here that such a systematic shift in PL peak position, especially for emission peaks below and above 785 meV [Figs. 7(a)–7(d)] as a function of fluence cannot be explained in light of defect-related radiative recombination of excitons as predicted earlier by several authors.[14–19]

We now give an account of the origin of GaSb nanocrystallites that remain embedded in the porous microstructure in order to understand the observed blue shift in PL emission. The processes that lead to the formation of a nanoporous layer containing nanofibers were discussed in detail in Ref. 12. In short, during the early stage of implantation, the vacancies created in GaSb due to ion energy loss agglomerate into voids. The voids grow in size with irradiation as the vacancies created by further ion irradiation migrate to the existing voids. Finally, the interconnections of the growing voids result in a porous structure. At the same time, redeposited sputtered atoms on top of the porous layer lead to the formation of patches or ridge-like structures. A continuous top surface is formed at higher fluences in case of off-normally incident ions because of much higher rate of redeposition. This mechanism of formation of nanoporous layer is associated with the presence of crystallites observed in the present experiment. When the nanoporous layer is formed, the incident ions dissipate very small amount of energy in the layer (only during their passage through the nano-dimensional GaSb remaining in the porous layer).[12] Since the porous layer in GaSb starts to form at ion fluence as low as $\sim 10^{14}$–10^{15} ions cm^{-2},[6–10] it can be expected that ion-beam induced amorphization of GaSb remains incomplete and leaves behind the nanocrystallites embedded in the amorphous nanofibrous structure. During subsequent stages of implantation, very small amount of the incident energy is deposited in the nanoporous layer, which is insufficient for complete amorphization of the embedded crystallites.[12]

IV. CONCLUSIONS

In summary, we report on detail morphological and microstructural studies along with vibrational properties and infrared luminescence of medium energy Ar^+-ion implantation induced porous GaSb in the high fluence regime ($7 \times 10^{16} - 3 \times 10^{18}$ ions cm^{-2}). Our studies demonstrate the presence of crystalline phases in the amorphous matrix of the nanoporous layer till the highest fluence of 3×10^{18} ions cm^{-2}. The nanoporous layer turns out to be oxidized with the existence of β-Ga_2O_3 on the surface of the nanostructures, and is also found to be luminescent in the infrared regime, presumably because of quantum confinement of excitons in GaSb nanocrystallites. Moreover, the observed blue shift of the deconvoluted PL bands is discussed in light of gap opening with decreasing GaSb nanocrystallite size as a function of ion fluence.

ACKNOWLEDGMENTS

Authors gratefully acknowledge helps received from Professor S. Varma, from Institute of Physics, Bhbaneswar for XPS studies, Professor S. Dhar, Department of Electronic Science, University of Calcutta, Kolkata for PL measurements, and Professor P. K. Sahoo, National Institute of Science Education and Research, Bhubaneswar, for extending SEM facility. Mr. S. K. Garg, SUNAG Lab, Institute of Physics is acknowledged for his help during implantations. Helps received from T. Basu and M. Kumar, SUNAG Lab, Institute of Physics during the experiments are also acknowledged.

[1]P. S. Dutta, H. L. Bhat, and V. Kumar, J. Appl. Phys. **81**, 5821 (1997).
[2]A. H. Chin, S. Vaddiraju, A. V. Maslov, C. Z. Ning, M. K. Sunkara, and M. Meyyappan, Appl. Phys. Lett. **88**, 163115 (2006).
[3]B. M. Borg, K. A. Dick, B. Ganjipour, M. E. Pistol, L. E. Wernersson, and C. Thelander, Nano Lett. **10**, 4080 (2010).
[4]Y. N. Guo, J. Zou, M. Paladugu, H. Wang, Q. Gao, H. H. Tan, and C. Jagadish, Appl. Phys. Lett. **89**, 231917 (2006).
[5]S. Schulz, M. Schwartz, A. Kuczkowski, and W. Assenmacher, J. Cryst. Growth **312**, 1475 (2010).
[6]N. Nitta, M. Taniwaki, Y. Hayashi, and T. Yoshiie, J. Appl. Phys. **92**, 1799 (2002).
[7]N. Nitta and M. Taniwaki, Phys. B: Condens. Matter **376–377**, 872 (2006).
[8]S. M. Kluth, J. D. Fitz Gerald, and M. C. Ridgway, Appl. Phys. Lett. **86**, 131920 (2005).
[9]P. Kluth, S. M. Kluth, B. Johannessen, C. J. Glover, G. J. Foran, and M. C. Ridgway, J. Appl. Phys. **110**, 113528 (2011).

[10]A. Perez-Bergquist, S. Zhu, K. Sun, X. Xiang, Y. Zhang, and L. Wang, Small **4**, 1119 (2008).
[11]X. Zhou, W. Guo, A. G. Perez-Bergquist, Q. Wei, Y. Chen, K Sun, and L. Wang, Nanoscale Res. Lett. **6**, 6 (2011).
[12]D. P. Datta, A. Kanjilal, S. K. Garg, P. K. Sahoo, D. Kanjilal, and T. Som, J. Appl. Phys. **115**, 123515 (2014).
[13]D. P. Datta, A. Kanjilal, S. K. Garg, P. K. Sahoo, B. Satpati, D. Kanjilal, and T. Som, Appl. Surf. Sci. **310**, 189 (2014).
[14]A. M. Smith and S. Nie, Acc. Chem. Res. **43**, 190 (2010).
[15]L. Tirado-Mejía, J. A. Villada, M. delosRíos, J. A. Peñafiel, G. Fonthal, D. G. Espinosa-Arbeláez, H. Ariza-Calderón, and M. E. Rodríguez-García, Physica B **403**, 4027 (2008).
[16]S. Iyer, S. Hegde, K. K. Bajaj, A. Abul-Fadl, and W. Mitchel, J. Appl. Phys. **73**, 3958 (1993).
[17]S. Iyer, L. Small, S. Hegde, K. K. Bajaj, and A. Abul-Fadl, J. Appl. Phys. **77**, 5902 (1995).
[18]A. Bosacchi *et al*., J. Cryst. Growth **150**, 844 (1995).
[19]K. Ploog, Y. Ohmori, H. Okamoto, W. Stolz, and J. Wagner, Appl. Phys. Lett. **47**, 384 (1985).
[20]M. Jeppsson *et al*., J. Cryst. Growth **310**, 5119 (2008).
[21]R. Callec, P. N. Favennec, M. Salvi, H. L'Haridon, and M. Gauneau, Appl. Phys. Lett. **59**, 1872 (1991).
[22]X-Ray diffraction database JCPDS-International Centre for Diffraction Data, 07-0215 (1998).
[23]A. Kanjilal, Nanotechnology **13**, 682 (2002).
[24]D. B. Williams and C. Barry Carter, *Transmission Electron Microscopy* (Springer, New York, 2009).
[25]I. Geppert, M. Eizenberg, A. Ali, and S. Datta, Appl. Phys. Lett. **97**, 162109 (2010).
[26]V. M. Bermudez, J. Appl. Phys. **114**, 024903 (2013).
[27]Y. Sun and M. Wu, J. Appl. Phys. **78**, 6691 (1995).
[28]H. K. Kim, J. H. Jung, and D. J. Choi, Thin Solid Films **520**, 6947 (2012).
[29]D. M. Zhernokletov, H. Dong, B. Brennan, M. Yakimov, V. Tokranov, S. Oktyabrsky, J. Kim, and R. M. Wallace, Appl. Phys. Lett. **102**, 131602 (2013).
[30]D. M. Murape, N. Eassa, J. H. Neethling, R. Betz, E. Coetsee, H. C. Swart, J. R. Botha, and A. Venter, Appl. Surf. Sci. **258**, 6753 (2012).
[31]S. G. Kim, H. Asahi, M. Seta, J. Takijawa, S. Emura, R. K. Soni, and S. Gonda, J. Appl. Phys. **74**, 579 (1993).
[32]J. H. Dias da Silva, S. W. da Silva, and J. W. Galzerani, J. Appl. Phys. **77**, 4044 (1995).
[33]Y. H. Gao, Y. Bando, T. Sato, Y. F. Zhang, and X. Q. Gao, Appl. Phys. Lett. **81**, 2267 (2002).
[34]P. Guha, S. Chakrabarty, and S. Chaudury, Physica B **23**, 81 (2004).
[35]R. Jangir *et al*., J. Appl. Phys. **112**, 034307 (2012).
[36]A. Khan, W. Jadwisienczak, and M. Kordesch, Physica E **35**, 207 (2006).
[37]B. D. Diwan and V. B. Dubey, AIP Conf. Proc. **1536**, 279 (2013).